Local phenomena of $(1-x)PbMg_{1/3}Nb_{2/3}O_3$-$xPbTiO_3$ single crystals ($0 \leq x \leq 0.38$) studied by Raman scattering

Aneta Slodczyk,[1,2] Philippe Daniel,[2] and Antoni Kania[1,*]

[1]*A. Chelkowski Institute of Physics, University of Silesia, Uniwersytecka 4, 40-007 Katowice, Poland*

[2]*Laboratoire de Physique de l'Etat Condensé (UMR CNRS No. 6087), Université du Maine, Avenue O. Messiaen, 72-085 Le Mans Cedex 9, France*

(Received 4 July 2007; revised manuscript received 17 March 2008; published 16 May 2008)

The study of $(1-x)PbMg_{1/3}Nb_{2/3}O_3$-$xPbTiO_3$ (PMN-PT) single crystals where x is 0, 0.09, 0.21, 0.28, 0.32, 0.35, and 0.38 was carried out with the use of x-ray, dielectric, and Raman scattering techniques in a wide temperature range. In this work, special attention was paid to the analysis of the Raman spectra. However, the results of the structural and dielectric studies were used to better interpret the Raman features. On the basis of the results of these studies, a phase diagram is given. The investigations confirmed that with the increase in the $PbTiO_3$ (PT) content the relaxor behavior becomes ferroelectric and that structural phase transitions of different types are observed. Raman studies were performed in a broad temperature range for all concentrations to understand the complex behavior of the PMN-PT system. The origin of the high temperature Raman spectra is considered in the whole concentration range and an origin of these spectra is proposed. For pure PMN and the solid solutions with a Ti content lower than 0.21, the 1:1 chemical order in the *B*-ion sublattice leads to the appearance of clusters with $Fm\bar{3}m$ symmetry. For higher PT contents, the high temperature Raman spectra seem to originate from the polar nanoregions of rhombohedral or tetragonal symmetry. All of the obtained Raman results are interpreted with the use of the group theory analysis. These results confirmed that the symmetries determined from the x-ray diffraction are average ones and play the role of a matrix in which nanoregions with a distinct local symmetry (generally monoclinic) are embedded. The analysis of the Raman spectra allowed us to determine the temperature and composition dependences of the Raman line frequencies, the reduced intensities, and the widths, providing clear evidence for the occurrence of the phase transitions. The anomalous behavior of the line width of some Raman lines related to the Pb ion vibrations pointed to the special role of Pb ion dynamics in the mechanism of phase transitions in the PMN-PT system.

DOI: 10.1103/PhysRevB.77.184114 PACS number(s): 77.84.Dy, 78.30.−j, 61.05.cp

I. INTRODUCTION

Due to their outstanding electromechanical properties,[1–3] lead magnesium niobiate–lead titanate solid solutions $(1-x)PbMg_{1/3}Nb_{2/3}O_3$-$xPbTiO_3$, i.e., $(1-x)$PMN-xPT or PMN-PT, which are formed between the relaxor $PbMg_{1/3}Nb_{2/3}O_3$ and the ferroelectric $PbTiO_3$, are being intensively studied at present. When properly orientated, their piezoelectric coefficients reach the highest values reported so far. Therefore, these materials are widely used as important devices in medicine, telecommunications, as well as in high technology and military industries. Since their physical behavior enormously varies, the PMN-PT solid solutions are also very interesting from the basic point of view. Despite very intensive research, these materials still require further systematic studies as the interpretations of the results obtained by different authors are inconsistent. Consequently, many of PMN-PT properties still remain unclear.

The PMN-PT solid solutions belong to the family of perovskite structure materials with the general formula ABO_3 (Fig. 1). The sublattice A is occupied by Pb^{2+} ions, while the B site is occupied by randomly distributed Mg^{2+}, Nb^{5+}, and Ti^{4+} ions. The phase diagram of the PMN-PT solid solutions has been already investigated by several authors.[4–9] According to the currently accepted zero field $(1-x)$PMN-xPT phase diagram,[6] four characteristic regions with different physical properties can be distinguished:

Region I—including pure PMN and solid solutions with Ti contents lower than 0.05 (Ref. 10).

Region II—the so-called rhombohedral, specific for solid solutions with Ti concentrations from 0.05 to 0.30.

Region III—the morphotropic phase boundary (MPB) region, including solid solutions with Ti contents from 0.31 to 0.37.

Region IV—the so-called tetragonal, for compositions with Ti contents higher than 0.38.

Region I can be well characterized by the classical relaxor behavior of $PbMg_{1/3}Nb_{2/3}O_3$. PMN possesses the cubic symmetry with the $Pm\bar{3}m(O_h^1)$ space group in the entire temperature range.[11] However, the results of numerous experiments such as x-ray and neutron diffraction,[12–16] neutron scattering,[17,18] transmission electron microscopy,[19–21] optical

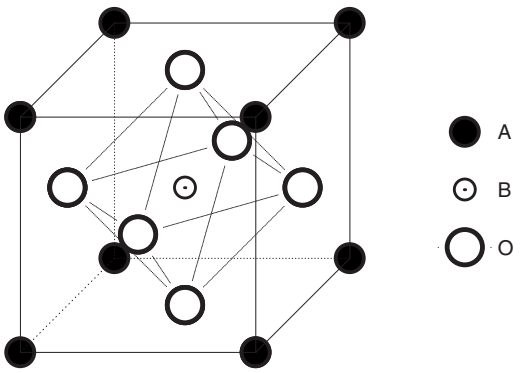

FIG. 1. The ABO_3 perovskite structure.

birefringence,[22] extended x-ray-absorption fine structure (EXAFS),[23] and NMR[24] revealed the presence of ordered regions, which are characterized by a local symmetry different from $Pm\bar{3}m$, embedded in the disordered cubic matrix. There are two types of these short ranged ordered regions: the clusters with the $Fm\bar{3}m$ space group and the polar nanoregions (PNRs) with the rhombohedral symmetry ($R3m$). The former originate from the chemical 1:1 order in the B sublattice, while the latter are the effect of the correlated ion off-center displacements.

The solid solutions from region II also exhibit a relaxor behavior; however, for these materials, the structural phase transition from the cubic ($Pm\bar{3}m$) to the rhombohedral ($R3m$) symmetry is observed.

Region III of the PMN-PT phase diagram, which is the MPB, is most commonly investigated since the crystals from this region exhibit the so-called giant piezoelectricity. In region III, the typical relaxor properties vanish and, thus, the solid solutions already tend to exhibit a ferroelectric behavior. Two structural phase transitions are observed for these materials. The first is from the cubic ($Pm\bar{3}m$) to the tetragonal ($P4mm$) symmetry, while the second is from the tetragonal to the monoclinic (Pm) one. However, the problem of symmetry in the MPB region seems to be more complex since the monoclinic symmetry can coexist with a secondary minority rhombohedral or tetragonal phase. Moreover, even the presence of a third minority orthorhombic phase cannot be ruled out. These different crystal structures observed in the vicinity of the MPB are energetically close to each other[25] and even a small external electric field may induce transition between them.[26,27]

The solid solutions from region IV of the PMN-PT phase diagram show a typical ferroelectric behavior. They undergo structural phase transition from the cubic $Pm\bar{3}m$ symmetry to the tetragonal $P4mm$ similarly as pure PT does.[28]

It should be stressed that even if the phase diagram described above is widely accepted, the structural properties of this system are still far from clear. Namely, Gehring *et al.*[7] and Xu *et al.*[29] suggested that the observed symmetry in solid solutions with a PT content lower than 0.27 depends on the radiation used in the experiments. The x-ray studies pointed to the rhombohedral symmetry, whereas the neutron experiments indicated a cubic one, thus suggesting that the symmetry of the outer layer is different from that of the bulk of crystals. This evidence of symmetry is called phase X. Additionally, some authors reported that the monoclinic symmetry is already observed for solid solutions with a PT content equal to 0.27 (Ref. 30) or 0.29.[8] Moreover, even the presence of two different monoclinic symmetries with Cm and Pm space groups in the vicinity of the MPB was proposed.[9,30] Therefore, the range of the MPB existence as well as the sequences of the observed phase transitions in the whole concentration range requires clarification. The solving of these problems seems to be difficult because PMN-PT solid solutions are highly disordered and inhomogeneous materials in which the coexistence of phases with different symmetries and different coherence lengths are found. Therefore, Raman spectroscopy, due to its sensitivity to local symmetry,[31,32] is a powerful technique in studying these materials.

Raman studies of PMN-PT solid solutions have already been performed by several authors. Husson *et al.*,[33] Siny *et al.*,[34,35] Jiang *et al.*,[36,37] and Svitelskiy *et al.*[38] carried out vibrational studies of pure PMN. $(1-x)$PMN-xPT with Ti contents of 0, 0.07, 0.10, and 0.13 were investigated by Idink and White,[39] while those with Ti contents of 0, 0.10, and 0.20 by Marssi *et al.*[40] Kamba *et al.*[41] performed Raman and IR reflectivity studies of 0.71PMN-0.29PT. The Raman spectra of PMN and compounds with 0.10 and 0.35 contents were studied under high pressure by Chaabane *et al.*[42] The temperature evolutions of the Raman spectra for the whole concentration range were done only by Ohwa *et al.*[43] However, in this study, some of the results were obtained by using single crystals and some by using ceramics. In spite of the fact that the Raman spectra obtained by different authors are similar, their interpretations are often contradictory.

It is worth stressing that the explanation of the origin of the complex Raman spectrum and assignment of the lines are a general problem of ferroelectric relaxors such as PMN, $PbZn_{1/3}Nb_{2/3}O_3$ (PZN),[44,45] disordered $PbSc_{1/2}Ta_{1/2}O_3$ (PST),[31,46,47] and $PbIn_{1/2}Nb_{1/2}O_3$ (PIN),[48] as well as PMN-PT and PZN-PT[49–51] solid solutions. One of the most interesting phenomena concerning these compounds is related to the presence of the first-order Raman spectrum within the cubic paraelectric phase. The origin of this spectrum has been explained in several ways. The widely accepted one postulates that the Raman spectrum originates from the nanoregions with the $Fm\bar{3}m$ space group, which appear due to 1:1 chemical order in the B sublattice.[46–48] However, as it has already been stated,[43,49,52] such a model can probably explain the presence of the Raman spectra for PMN-PT with a small PT content only.

The temperature evolution of the Raman spectra of PMN-PT in the whole concentration range has not been well described yet. Upon temperature change, these Raman spectra slightly differ. Both at high and low temperatures, their Raman modes are very broad and overlapping. This high complexity of the Raman spectra makes their assignment and interpretation difficult. Hence, most authors have presented only qualitative analyses for selected compositions. There is an apparent lack of a quantitative analysis of Raman spectra for the PMN-PT system. A complex analysis of temperature dependences of the Raman spectra based on the multiple peak decomposition for pure PMN was only offered by Svitelskiy *et al.*[38]

Therefore, the explanation of the origin of high temperature Raman spectra in the whole concentration range and the analysis of the temperature evolution of the Raman spectra for $(1-x)$PMN-xPT solid solutions where $0 \leq x \leq 0.38$ are the main goals of this paper. In order to fulfill these aims, structural, dielectric, and Raman studies of PMN-PT single crystals in a wide temperature range were carried out. Complementary investigations performed on single crystals from the same crystal growth processes covering a wide concentration range enabled us to present a global view of this system. In particular, we focused on a detailed analysis of the Raman spectra. In order to better interpret the Raman scattering data, we used our own structural and dielectric results. The calculations based on the independent damped oscillator

model allowed us to determine the number of active modes within each characteristic symmetry for all of the investigated samples and compare them to the group theory prediction. Additionally, with the use of this model temperature and composition dependences of wave numbers, reduced intensities and line widths were obtained. The Raman studies made the investigation of the local phenomena possible. They constitute the key to the understanding of the physics of the PMN-PT system, for example, the Pb ion dynamics and its important role in the physics of ferroelectric relaxors. The presented studies provide important information for a better understanding of the complicated behavior of the PMN-PT system.

II. EXPERIMENTAL METHODS

The studied PMN-PT single crystals were grown by the flux method. The PbO-Pb_3O_4-B_2O_3 system was used as the solvent. The crystallization processes were carried out in the temperature range from approximately 1100 °C to approximately 900 °C. Yellow, transparent, and rectangular shaped single crystals of size up to $6\times6\times4$ mm^3 were obtained. The actual composition of the grown crystals were determined by energy dispersive x-ray spectroscopy (EDS) and using a JSM-5410 JEOL scanning electron microscope. More details concerning the crystal growth procedure have been published elsewhere.[53]

X-ray powder diffraction measurements were performed by using the high-resolution Siemens D5000 diffractometer (θ-2θ geometry, filtered Cu $K\alpha$ radiation, $V=40$ kV, and $I=30$ mA). In order to determine the crystal symmetry and the temperature of phase transitions, the scans [$|\Delta(2\theta)|=0.01°$, counting time 10 s] of the selected Braggs reflections, (100), (110), (111), (200), (220), (211), and (310), were collected in a wide temperature range. Additionally, at several chosen temperatures, the full pattern in the range of $18°-120°$ was recorded by using the scanning method with a step $|\Delta(2\theta)|=0.02°$ and a counting time of 10 s. For these temperatures, the crystal structure refinements were performed by using the profile Rietveld method by means of the FULLPROF software.

Single crystals for dielectric measurements were cut parallel to the (100) natural faces, polished, and electroded with silver paste. Dielectric measurements were performed by using HP 4263B LCR Meter for frequencies of 0.1, 1, 10, and 100 kHz and measuring an electric field of about 20 V cm^{-1}. Measurements were carried out within the temperature range from 110 to 570 K.

The Raman spectra were collected by using a T64000 Yvon-Jobin multichannel triple monochromator spectrometer equipped with a charge coupled device detector (micro-Raman configuration, backscattering geometry). The 488 and 514 nm argon ion laser excitation lines were selected. The measurements were performed in a temperature range from 77 to 700 K. The Raman spectra were recorded in the 25–1000 cm^{-1} range. The PEAKFIT software program by Jandel Scientific was used to deconvolute overlapping modes and to determine the characteristic parameters of lines such as integrated intensity, full width at half maximum, and peak position.

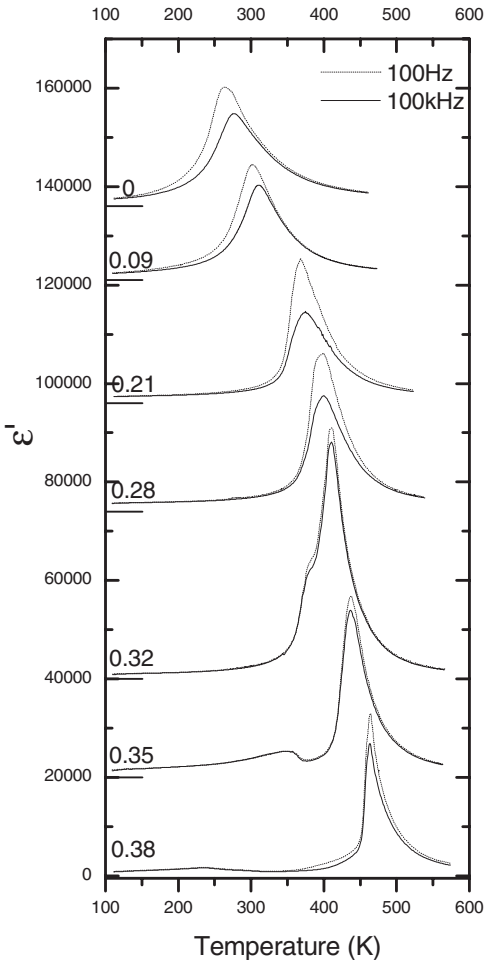

FIG. 2. Temperature dependences of the real parts of the dielectric permittivity for $(1-x)$PMN-xPT $(0\leq x\leq 0.38)$ single crystals.

III. RESULTS AND DISCUSSION

A. X-ray and dielectric results

Figure 2 presents the temperature dependences of the real part of the dielectric permittivity for the investigated single crystals $(0\leq x\leq 0.38)$. For clarity of the picture, these dependences are only shown for two frequencies: 100 Hz and 100 kHz. As can be seen, the increase in the PT content changes the nature of the observed phase transitions and shifts the $\varepsilon(T)$ maxima toward higher temperatures. The structural properties of the PMN-PT are also strongly composition dependent. Therefore, the analysis of the temperature evolution of Bragg's reflections together with the crystal structure refinements allowed us to determine the symmetries and the temperature of the observed structural phase transitions. It is noteworthy that the structural analysis revealed the presence of diffuse scattering for all of the investigated compositions. Diffuse scattering appears with the cubic symmetry and is also observed within lower symmetries. Moreover, for some solid solutions (Fig. 3), the diffuse scattering is very strong, especially at low temperatures. The occurrence of diffuse scattering can be related to the presence of polar nanoregions with different symmetries and, therefore, it suggests that the symmetries determined from the x-ray

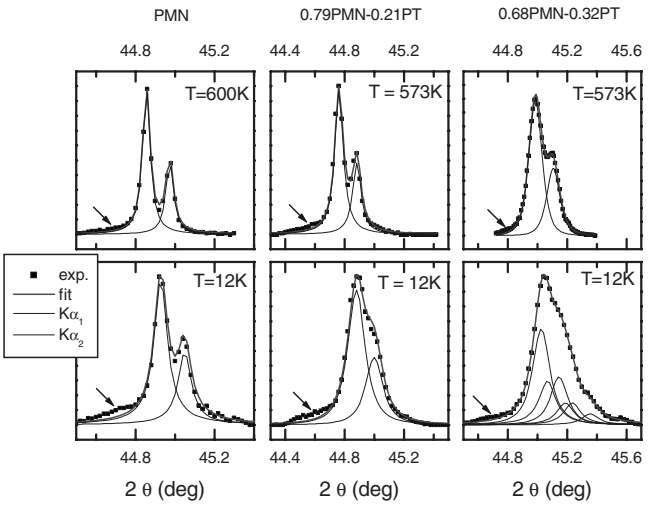

FIG. 3. Temperature evolution of the (200) Bragg reflection for PMN, 0.79PMN-0.21PT, and 068PMN-0.32PT solid solutions at high and low temperatures. The arrows mark the presence of diffuse scattering.

studies are only averaged. Our x-ray and dielectric results are summarized in the phase diagram presented in Fig. 4. The characteristic temperatures deduced from the Raman scattering studies are also included. This phase diagram is in good agreement with the one determined by Noheda *et al.*[6] and, thus, it can be similarly divided into three regions with distinct structural and dielectric properties.

Region I is represented by PMN, which shows the classical relaxor behavior. According to our x-ray studies, PMN possesses a cubic symmetry with the $Pm\bar{3}m$ space group in the measured temperature range. However, the occurrence of diffuse scattering (Fig. 3) and the departure from the linear dependence of the lattice parameters versus temperature, as well as the departure from the Curie–Weiss law observed below 600 K, point to the appearance of polar nanoregions within the cubic symmetry.

The 0.91PMN-0.09PT, 0.79PMN-0.21PT, and 0.72PMN-0.28PT solid solutions belong to region II. The dielectric

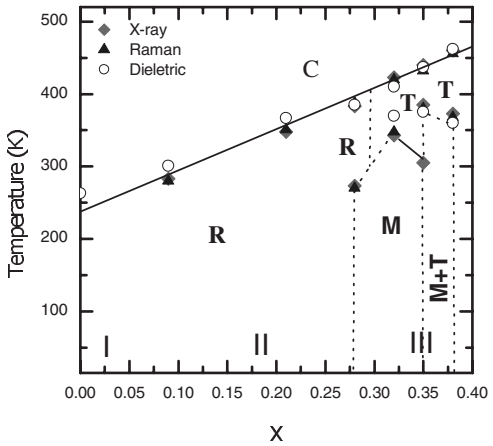

FIG. 4. Phase diagram of the $(1-x)$PMN-xPT $(0 \leq x \leq 0.38)$ determined from the complementary x-ray, dielectric, and Raman scattering studies.

results show that these materials also exhibit the relaxor behavior. However, as can be seen in Fig. 2, with an increase in the Ti content, the characteristic relaxor properties become weaker. It is noteworthy that in the cases of 0.79PMN-0.21PT and 0.72PMN-0.28PT, the dielectric dispersion is observed on both sides of the $\varepsilon(T)$ maximum. Unlike PMN, the solid solutions from this region exhibit the structural phase transition. The 0.91PMN-0.09PT, 0.79PMN-0.21PT, and 0.72PMN-0.28PT undergo a transition from the cubic $(Pm\bar{3}m)$ to the rhombohedral symmetry $(R3m)$ at 283, 348, and 383 K, respectively. For 0.72PMN-0.28PT, the additional phase transition from the rhombohedral to the monoclinic symmetry (Pm) is observed at 273 K. The existence of two phase transitions for this sample is not consistent with the phase diagram of Noheda *et al.*[6] However, the presence of the monoclinic symmetry for composition x equal to 0.27 and 0.295 has been previously shown in other works.[8,30] The departures both from the linear dependence of the lattice parameters versus temperature and from the Curie–Weiss law are also observed. These results show that below 450, 480, and 520 K, the polar nanoregions play an important role and affect all properties of 0.91PMN-0.09PT, 0.79PMN-0.21PT, and 0.72PMN-0.28PT, respectively. As it already stated in a previous paper,[52] it is almost certain that the rhombohedral phase below T_c is not a long range order property and is still limited to clusters that are large enough to be detected by x-ray diffraction. The fact that these materials can achieve the long range ferroelectric polar order only when the external electric field is applied seems to confirm this hypothesis.

The 0.68PMN-0.32PT, 0.65PMN-0.35PT, and 0.62PMN-0.38PT solid solutions belong to region III, i.e., the MPB region. For these materials, the dielectric dispersion significantly diminishes and the temperature of the $\varepsilon(T)$ maximum becomes frequency independent. Therefore, their dielectric properties can already be classified as ferroelectric ones. It is worth stressing that temperature dependences of the dielectric permittivity reveal, except for the main $\varepsilon(T)$ maximum related to the cubic $(Pm\bar{3}m)$-tetragonal $(P4mm)$ phase transition, the presence of a second characteristic anomaly connected with the tetragonal-monoclinic (Pm) transition. The x-ray results show that the first transition takes place at 423, 440, and 460 K for 0.68PMN-0.32PT, 0.65PMN-0.35PT, and 0.62PMN-0.38PT, respectively. The second is observed at 343, 385, and 373 K for 0.68PMN-0.32PT, 0.65PMN-0.35PT, and 0.62PMN-0.38PT, respectively. However, 0.65PMN-0.35PT and 0.62PMN-0.38PT structurally differ from 0.68PMN-0.32PT since these two solid solutions exhibit a region of coexistence of the tetragonal and monoclinic phases. In the case of 0.65PMN-0.35PT, this coexistence is observed in the temperature range 385–305 K, while for 0.62PMN-0.38PT, the region of such coexistence extends from 373 to 12 K. For all materials from region III, the presence of diffuse scattering and the departures from both the linear dependence of the lattice parameters versus temperature and the Curie–Weiss law were revealed below 550 K. These characteristic features point to the existence of PNRs.

The crystal structure refinement performed for all of the investigated solid solutions shows that the considered rhom-

TABLE I. The main results of the crystal structure refinements performed for $(1-x)$PMN-xPT $(0 \leq x \leq 0.38)$ solid solutions at selected temperatures.

Compound	T (K)	Space group	Reliability factors (%)	B_{Pb}^{iso} (Å^2)
PMN	650	$Pm\bar{3}m$	$R_{Bragg}=8.24$, $R_F=8.11$	3.76
	300	$Pm\bar{3}m$	$R_{Bragg}=9.03$, $R_F=8.77$	4.33
	12	$Pm\bar{3}m$	$R_{Bragg}=8.97$, $R_F=8.94$	3.98
0.91PMN-0.09PT	300	$Pm\bar{3}m$	$R_{Bragg}=7.98$, $R_F=8.02$	4.21
	12	$R3m$	$R_{Bragg}=7.04$, $R_F=7.22$	2.37
0.79PMN-0.21PT	598	$Pm\bar{3}m$	$R_{Bragg}=8.97$, $R_F=9.11$	4.38
	300	$R3m$	$R_{Bragg}=8.59$, $R_F=8.33$	3.94
	12	$R3m$	$R_{Bragg}=8.14$, $R_F=7.94$	3.46
0.72PMN-0.28PT	605	$Pm\bar{3}m$	$R_{Bragg}=8.42$, $R_F=8.88$	4.43
	300	$R3m$	$R_{Bragg}=8.76$, $R_F=7.92$	3.92
	12	Pm	$R_{Bragg}=7.11$, $R_F=6.94$	2.27
0.68PMN-0.32PT	650	$Pm\bar{3}m$	$R_{Bragg}=8.76$, $R_F=8.48$	4.49
	383	$P4mm$	$R_{Bragg}=7.97$, $R_F=7.99$	3.88
	12	Pm	$R_{Bragg}=7.12$, $R_F=6.99$	2.70
0.65PMN-0.35PT	673	$Pm\bar{3}m$	$R_{Bragg}=8.79$ $R_F=8.97$	4.52
	410	$P4mm$	$R_{Bragg}=8.11$, $R_F=8.05$	3.61
	353	$P4mm+Pm$	$R_{Bragg}=7.55$, $R_F=7.41$	2.92
			$R_{Bragg}=6.98$, $R_F=7.07$	2.53
	12	Pm	$R_{Bragg}=6.82$, $R_F=6.95$	2.04
0.62PMN-0.38PT	673	$Pm\bar{3}m$	$R_{Bragg}=8.23$, $R_F=8.18$	4.39
	423	$P4mm$	$R_{Bragg}=7.85$, $R_F=7.98$	3.58
	12	$P4mm+Pm$	$R_{Bragg}=7.26$, $R_F=7.32$	2.07
			$R_{Bragg}=6.78$, $R_F=6.97$	1.88

bohedral ($R3m$), tetragonal ($P4mm$), and monoclinic (Pm) crystal structures are very similar. This suggests that they are energetically very close to each other and, thus, the transitions between them are relatively simple. It must be pointed out that the determined values of the reliability factors (R_{Bragg} and R_F) and the isotropic thermal factors for Pb ions (B_{Pb}^{iso}) are very high. These values are listed in Table I. Such high values of B_{Pb}^{iso} are often observed for lead based perovskites[16,30,54–57] and are usually explained by disorder in the Pb ion displacement. Therefore, these results show that both high and low temperature phases of the PMN-PT system are highly disordered. It is noteworthy that our x-ray photoelectron spectroscopy studies show the presence of the highest structural disorder in the vicinity of the MPB.[58] As described above, the structural and dielectric studies point to the presence of polar nanoregions. Hence, the crystal structures determined from x-ray studies are only average and play the role of a matrix in which these short range ordered clusters with different local symmetries are embedded. With temperature decrease, the PNRs grow and may lead to phase transition. Thus, the observed phase transitions are the effect of the correlated ion off-center displacements. The high values of B_{Pb}^{iso} point to the special role of Pb ions in the phase transition mechanism. Similar results were presented by Dkhil *et al.*[16] and Slodczyk *et al.*[52] in the case of PMN, 0.9PMN-0.1PT, and 0.91PMN-0.09PT.

Our dielectric and structural results showed that the PMN-PT solid solutions are disordered and nonhomogeneous materials. However, it should be stressed that values of the R_{Bragg} and R_F as well as of B_{Pb}^{iso} have a tendency to decrease with the increase in the PT content. This shows that the increase in Ti content enhances the development of the long range order in this system.

B. Raman scattering results

Attempts at recording polarized Raman spectra for the crystals studied here were undertaken but proved to be unsuccessful. This was probably caused by the presence of the complex structure resulting from differently oriented PNRs (for small Ti contents) or fine domains (for higher Ti contents). Therefore, in further investigations, unpolarized Raman spectra were collected. Figure 4 presents the unpolarized Raman spectra of the $(1-x)$PMN-xPT single crystals where the composition x is 0, 0.09, 0.21, 0.28, 0.32, 0.35, 0.38, 0.50, and 0.64 as recorded at 77 and 700 K. Note that these Raman spectra as well as the following ones presented in this paper were corrected by using the Bose–Einstein population factor.

The Raman spectra presented in Fig. 5 are similar to those previously presented by different authors.[33–43] They also consist of a number of broad lines, even at 77 K, and they are observed in the whole measured temperature range. Since this is quite commonly found in oxide perovskites, such Raman characteristics could indicate the presence of a second-order Raman contribution. However, note that generally, the second-order Raman spectra closely resembles the phonon density of states (with an expanded scale), which involves a higher width of lines, especially in disordered materials. Nevertheless, this phenomenon is not observed here. Moreover, the coexistence of both first- and second-order Raman spectra could also be possible. However the temperature dependences of the Raman line intensities, i.e., the decrease in intensities with temperature increase (see Fig. 16), as well as the lack of Raman bands above 900 cm^{-1} seem to indicate that the investigated Raman spectra are probably mainly of the first order. Even if the possibility of a second-order contribution cannot be completely brushed aside, our observations are in good agreement with literature data.[33–36,38,39]

The PMN-PT Raman spectra can be divided into three characteristic regions of frequency: the low frequency region, which is approximately up to 150 cm^{-1}; the intermediate frequency region, which is approximately from 150 to 500 cm^{-1}; and the high frequency region, which is from 500 to 800 cm^{-1}. According to the attempts of mode assignment in the case of PMN[33] and especially due to lattice dynamics calculations performed by Prosandeev *et al.*,[59] the low frequency region can be attributed to the Pb-BO_6 stretching modes. The modes from the intermediate frequency region can be classified as mixed B-O-B bending and O-B-O stretching, while those from the high frequency region as B-O-B stretching.

The Raman spectra shown in Fig. 5 seem to be similar to each other, especially those recorded at high temperatures.

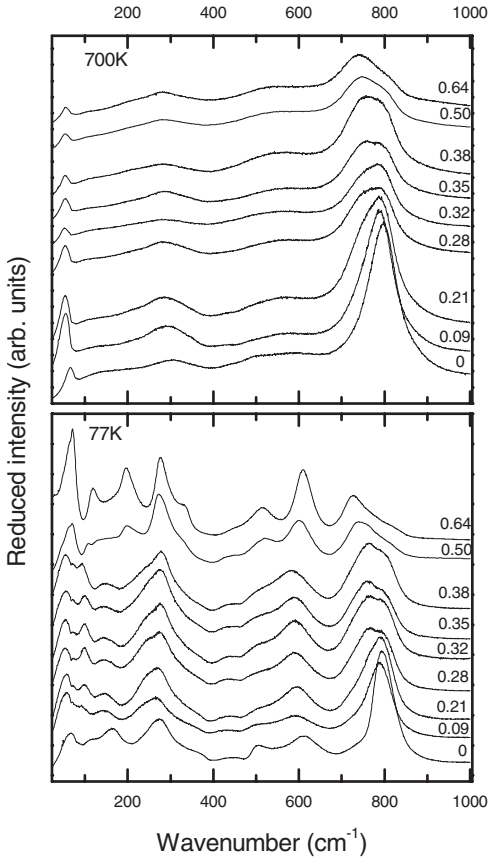

FIG. 5. Unpolarized Raman spectra of the $(1-x)$PMN-xPT $(0 \leq x \leq 0.64)$ solid solutions presented at 700 and 77 K.

However, even the qualitative analysis reveals noticeable changes in these Raman spectra versus the PT content. At 700 K the most significant difference is related to the presence of a new line near the highest frequency mode that appears for the concentration $x \geq 0.21$. The Raman spectra collected at 77 K exhibit more evident differences that can be seen in the entire frequency range and in the linewidths of the observed modes. These distinguishing features suggest that three kinds of behavior versus concentration exist, for which the origin and the interpretation of the Raman spectra are different. The first one is characteristic of pure PMN (region I), the second for the solid solutions from regions II and III, whereas the third one is for the crystals from region IV. These characteristic regions in which the Raman spectra are quite similar are consistent with those determined from the dielectric and structural results.

As it has already been mentioned, in this paper we focus on regions I–III, i.e., $0 \leq x \leq 0.38$. In order to determine the origin and interpret the Raman spectra, a full group theory analysis was performed. The calculations of the normal vibrational modes for all of the symmetries observed in these materials were done by using the site symmetry method. The results are presented in Table II.

1. High temperature Raman spectra

As it can be clearly seen in Fig. 5, all of the investigated PMN-PT solid solutions possess first-order Raman spectra at 700 K. At this temperature, the symmetry of each material is cubic with the $Pm\bar{3}m$ space group. According to the group theory analysis, first- order Raman modes are not allowed for such a symmetry. Moreover, the presence of the Raman spectrum within the high temperature paraelectric phase is not typical either of PMN-PT or PZN-PT systems. First-order Raman spectra were observed in many complex perovskites. The Raman studies of PST[46,47] and PIN[48] with a different degree of order in the B-ion sublattice reveal that their Raman spectra are associated with the existence of the 1:1 order in the B sublattice. Such order leads to the doubling of the unit cell and in consequence to the cubic symmetry with the $Fm\bar{3}m$ space group. For this symmetry, there are four allowed active Raman modes. Experimentally, three main modes located near 50, 350, and 800 cm^{-1} are detected for these materials.

The origin of the high temperature Raman spectra of PMN and 0.91PMN-0.09PT can also be explained by the existence of the 1:1 chemical order. It should be stressed that the presence of such order in these materials was experimentally proved and can be well described within the framework of the charged balanced random layer model.[19–21,60] The Raman spectra of both PMN and 0.91PMN-0.09PT exhibit three main lines of the first-order character located near 50, 280, and 790 cm^{-1}. Additionally, two broad bands near 160 and 550 cm^{-1} are observed. Due to very high values of their linewidths, it cannot be excluded that they are of the second-order character. However, it is possible that these bands can also exhibit the first-order character as it was previously stated,[38] but in that case their origin can be related to the nucleation of the polar nanoregions. Therefore, the unambiguous assignment of the observed lines at 700 K is not

TABLE II. Group theory analysis for each of characteristic symmetry. The calculations were done at the center of the Brillouin zone—the Γ point.

Symmetry	Γ_{tot}	Γ_{Raman}
$Pm\bar{3}m(O_h^1)$	$\Gamma=3F_{1u}+F_{2u}+F_{1u}$	$\Gamma_{Raman}=0$
$Fm\bar{3}m(O_h^5)$	$\Gamma=A_{1g}+E_g+2F_{2g}+F_{1g}+5F_{1u}+F_{2u}$	$\Gamma_{Raman}=A_{1g}+E_g+2F_{2g}$
$R3m(C_{3v}^5)$ $(Z=1)$	$\Gamma=4A_1+A_2+5E$	$\Gamma_{Raman}=3A_1+4E$
$R3m(C_{3v}^5)$ $(Z=2)$	$\Gamma=8A_1+2A_2+10E$	$\Gamma_{Raman}=7A_1+9E$
$Pm(C_S^1)$	$\Gamma=10A_1+5A_2$	$\Gamma_{Raman}=8A_1+4A2$
$P4mm(C_{4v}^1)$	$\Gamma=4A_1+B_1+5E$	$\Gamma_{Raman}=3A_1+B1+4E$

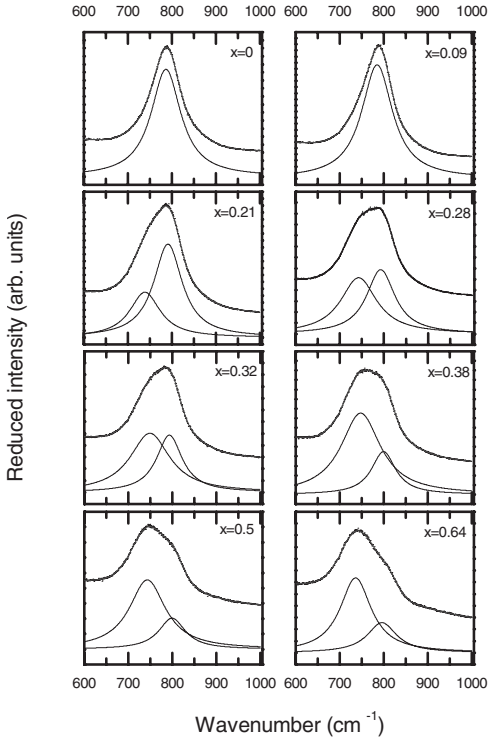

FIG. 6. Composition $(0 \leq x \leq 0.64)$ evolution of the components of the Raman mode located near 790 cm^{-1} at 700 K.

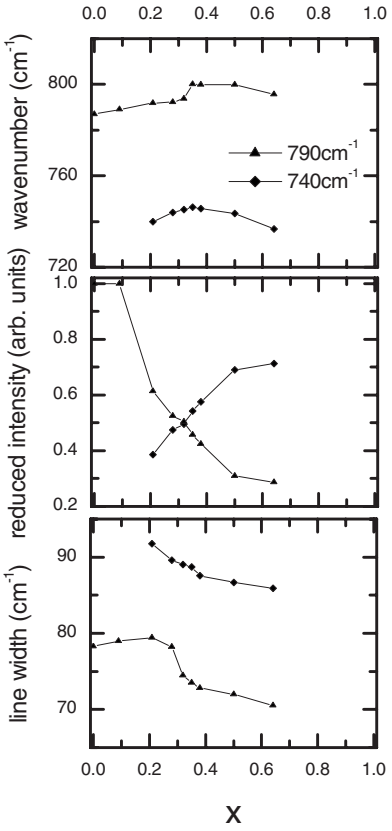

FIG. 7. Composition $(0 \leq x \leq 0.64)$ dependences of the wave numbers, reduced intensities, and linewidths of the components of the Raman modes located near 790 cm^{-1} at 700 K.

possible. Prosandeev *et al.*[59] also pointed out that even if phonons in PMN should be very broad due to disorder, some of the experimentally observed lines exhibit an unexpectedly small damping constant.

It seems hardly possible for the 1:1 chemical order to be present in the whole composition range in the PMN-PT system. Therefore, a new origin of the presence of Raman spectra at high temperatures should be considered. As can be seen from Fig. 5, with the increase in Ti content the Raman modes become narrower and a new mode near 740 cm^{-1} appears. Moreover, the Raman modes located near 280 and 550 cm^{-1} are not longer symmetric and, thus, in order to properly fit the spectra, additional lines must be introduced. It is worth noting that these features are a clear indication of a change in the local symmetry. From the symmetry point of view, the composition behavior of the mode located near 790 cm^{-1} is especially sensitive to the changes in the crystal symmetry.[34,37] Figure 6 presents the evolution of components of this Raman line for the composition $0 \leq x \leq 0.64$. A similar composition behavior of this high frequency line was presented by Ohwa *et al.*[43] and Iwata *et al.*[49] for PMN-PT and PZN-PT, respectively. They observed that the superstructure reflections $\{\frac{h}{2}\frac{k}{2}\frac{l}{2}\}$, which are the effect of the 1:1 order, vanish for PT contents higher than 0.2, while the Raman spectra disappear only for the composition when x equals 0.8. On the basis of these results, they also suggested that the 1:1 chemical order cannot be responsible for the Raman spectrum presence in the considered range $0 \leq x \leq 0.8$. They stated that a new origin of the Raman spectra for materials with higher PT contents should be considered but no explicit one was proposed.

The composition dependences of the wave numbers, reduced intensities, and linewidths of the Raman A_{1g} mode near 790 cm^{-1} are shown in Fig. 7. As it is clearly seen in Figs. 6 and 7, for PMN and the solid solutions with low Ti contents (up to 0.09), this mode is single, which is in good agreement with the predictions for the $Fm\bar{3}m$ symmetry. Starting with the crystals wherein the Ti content equals 0.21, the new line appears near 740 cm^{-1}. The presence of two Raman modes in the frequency range 700–800 cm^{-1} seems to exclude the possibility of describing the symmetry by the $Fm\bar{3}m$ space group. Hence, the one possible solution is that the high temperature Raman spectra of $(1-x)$PMN-xPT solid solutions where $x \geq 0.21$ originate from the polar nanoregions with a symmetry different from $Fm\bar{3}m$. It seems reasonable to assume that the symmetries of these nanoregions are the same as the ones that appear below the structural phase transitions. It must be pointed out that the concentration dependences of both the frequencies and the linewidths exhibit the characteristic jumps observed in the range 0.28–0.32. It is probable that these jumps can indicate the changes in the local symmetry from the rhombohedral $R3m$ to the tetragonal $P4mm$. The results presented by Iwata *et al.*[49] for PZN-PT solid solutions showing the dependence of disappearance temperatures of the first-order Raman spectra versus concentration seem to confirm our suggestion. These authors revealed that in the case of materials with PT contents equal to 0.6 and 0.7, the Raman spectra vanish at approximately 920 and 820 K, respectively. Therefore, it is very difficult to expect that in these temperatures the order-

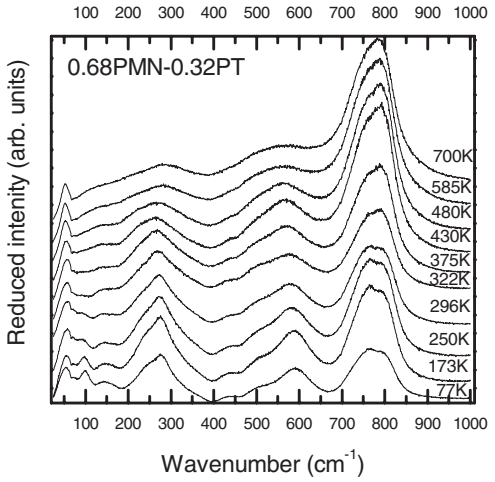

FIG. 8. Temperature evolution of the Raman spectra of 0.68PMN-0.32PT.

disorder transformation in the *B*-ion sublattice occurs since these temperatures are much lower than the ones well known for lead based complex perovskites.[61] If our proposal of high temperature Raman spectrum origin based on the presence of polar nanoregions is correct, then it indicates that the polar nanoregions appear at higher temperatures than those at which the departures from both the linear dependence of the lattice parameters versus temperature and from the Curie–Weiss law are observed.

The features presented in Figs. 6 and 7 point to the existence of three regions with different origins of the high temperature Raman spectrum. In the first region, which is characteristic of composition x from 0 to 0.09, the 1:1 chemical order is responsible for the presence of the Raman spectrum. In the second region, where x is from 0.21 to 0.28, the Raman activity originates from the polar nanoregions with the rhombohedral symmetry; while in the third one, which is for $x \geq 0.32$, the Raman activity is from the polar nanoregions of the tetragonal symmetry.

2. Temperature evolution of the Raman spectra

In general, the observed Raman spectra of the PMN-PT single crystals do not vary much with temperature. Figure 8 shows, for example, the Raman spectra of 0.68PMN-0.32PT recorded in a wide temperature range. The changes in these spectra are associated with the splitting of the Raman lines present at high temperatures and with the appearance of several new lines below 500 K.

It is worth noting that a precise determination of the quantitative changes in the spectra versus temperature for the investigated compound was only possible after calculations. The model of independent damped oscillators was used to deconvolute the Raman spectra and to determine the reduced intensity, frequency, and linewidth of each Raman mode. According to this model the intensity of Raman spectrum can be written in the form

$$I(\omega) = \frac{S_i \Gamma_i \omega_{i0}^2 \omega}{(\omega^2 - \omega_{i0}^2)^2 + \Gamma_i^2 \omega_{i0}^2}[n(\omega) + 1], \qquad (1)$$

where S_i, Γ_i, and ω_{i0} are the intensity factor, damping constant, and the mode frequency, respectively, while $n(\omega)$ is the

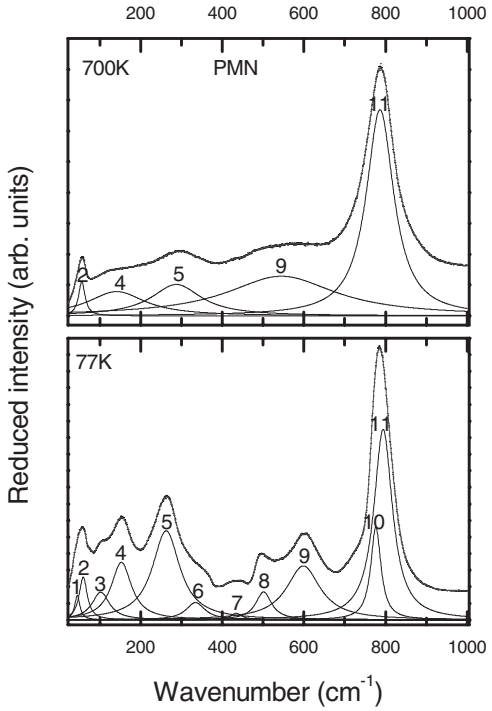

FIG. 9. Deconvolution of the Raman spectra of PMN at several selected temperatures. The numbers 1–11 label 11 Raman modes observed at 77 K. At high temperatures, this numeration is kept.

Bose–Einstein population factor. For every investigated crystal, the Raman modes are best resolved at low temperatures. Therefore, we began the fitting process with the spectrum recorded at the lowest temperature. The best fit in the preceding temperature was taken as the initial data for the next temperature. It is worth noting that for all of the investigated materials, very good agreement between the calculated and experimental spectra were obtained.

The examples of the deconvoluted Raman spectra of PMN, 0.79PMN-0.21PT, 0.72PMN-0.28PT, 0.68PMN-0.32PT, and 0.62PMN-0.38PT at several characteristic temperatures are presented in Figs. 9–13. The temperatures and compositions were chosen in such a way that they allowed us to show the Raman spectra for all of the symmetries existing in the investigated PMN-PT crystals.

The deconvolutions of the Raman spectra of PMN are presented in Fig. 9. At 700 K its spectrum is decomposed into five lines among which three are certainly of the first order. As it has already been discussed, this Raman spectrum originates from clusters with the $Fm\bar{3}m$ symmetry (see Sec. III B 1). Below the Burns temperature, i.e., 600 K, some modes split and a few new lines appear. These new features result from the existence of the polar nanoregions of the rhombohedral symmetry ($R3m$). Upon cooling, the Raman modes become narrower and more intense. This phenomenon is in very good agreement with the observed diffuse scattering (Fig. 3) and proves that the polar nanoregions grow with the decrease in temperature. Finally at 77 K, the Raman spectrum consists of 11 Raman modes. For the $R3m$ symmetry, the group theory analysis predicts seven active Raman lines. However, due to the existence of the 1:1 order in PMN,

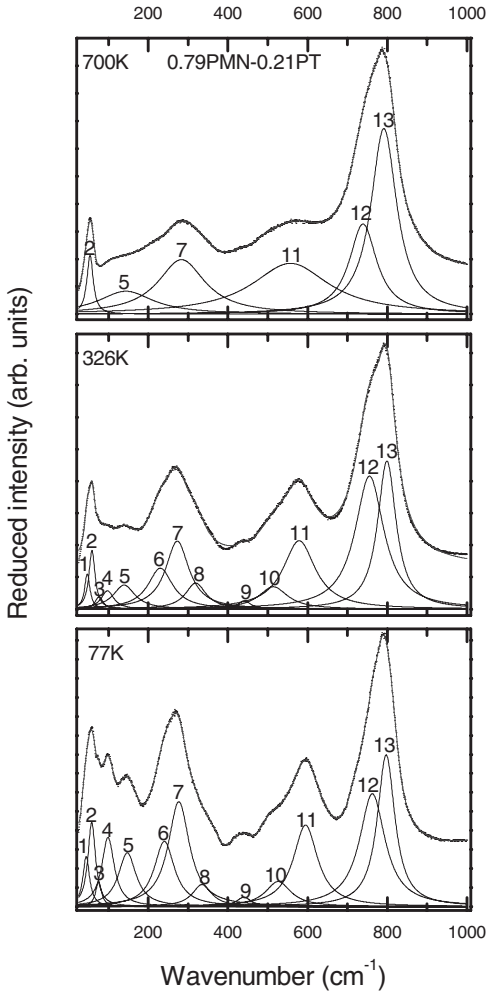

FIG. 10. Deconvolution of the Raman spectra of 0.79PMN-0.21PT at several selected temperatures. The numbers 1–13 label 13 Raman modes observed at 77 K. At high temperatures, this numeration is kept.

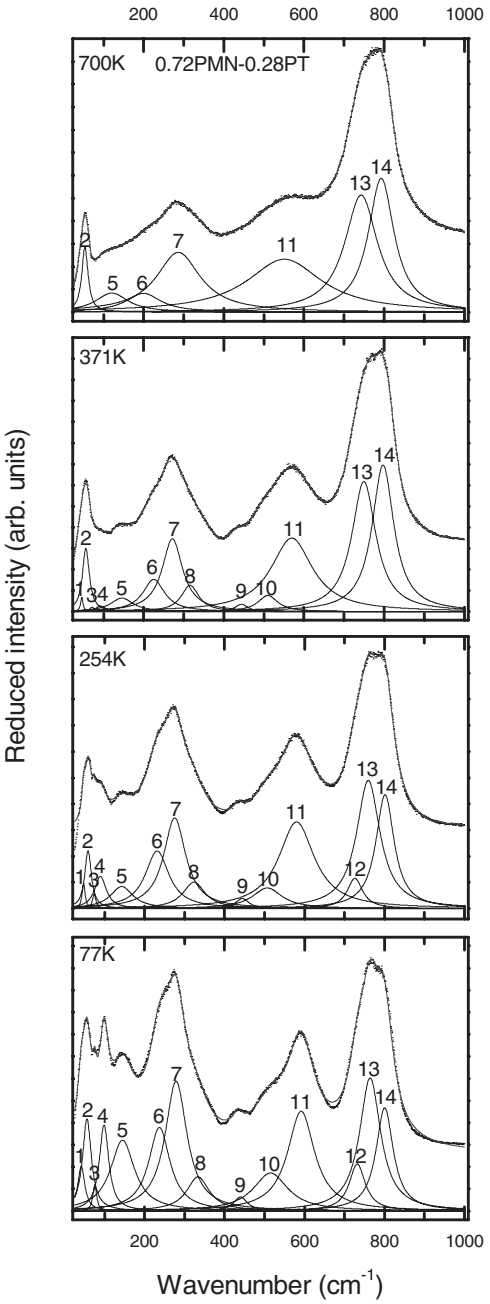

FIG. 11. Deconvolution of the Raman spectra of 0.72PMN-0.28PT at several selected temperatures. The numbers 1–14 label 14 Raman modes observed at 77 K. At high temperatures, this numeration is kept.

the $R3m$ symmetry with $Z=2$ should be considered here. In this case, 16 active Raman lines are allowed; however, we observed only 11 Raman lines. The differences between the numbers of observed and theoretically predicted modes can be explained by the fact that PMN is a highly disordered material. This disorder causes the broadening of the Raman lines and this together with the overlapping makes it impossible to distinguish all of them. Therefore, as similarly done in our previous studies,[38] we maintain that the Raman spectra of PMN originate from the 1:1 chemical order and the $Fm\bar{3}m$ (above the Burns temperature) and the $R3m$ (under the Burns temperature) local symmetries related to it.

The deconvoluted Raman spectra of the 0.79PMN-0.21PT and 0.72PMN-0.28PT solid solutions are shown in Figs. 10 and 11, respectively. The Raman spectra recorded at 700 K can be well decomposed into six lines for 0.79PMN-0.21PT and into seven lines in the case of 0.72PMN-0.28PT. As it has been postulated, the high temperature spectra of these materials come from the polar nanoregions of the rhombohedral symmetry ($R3m$). With the decrease in temperature, the splitting of some modes and the appearance of new ones are observed below 600 K. The most significant changes in the Raman spectra for both materials appear in the vicinity of the cubic-rhombohedral phase transitions (348 K for 0.79PMN-0.21PT and 383 K for 0.72PMN-0.28PT). It is worth noting that the Raman spectra do not significantly change during the additional rhombohedral-monoclinic phase transition observed for 0.72PMN-0.28PT at 273 K. Within the rhombohedral symmetry, the Raman spectra of both materials are deconvoluted into 13 lines, whereas the Raman spectra of 0.72PMN-0.28PT within the monoclinic symmetry into 14 lines. The group theory analysis predicts 7 active Raman

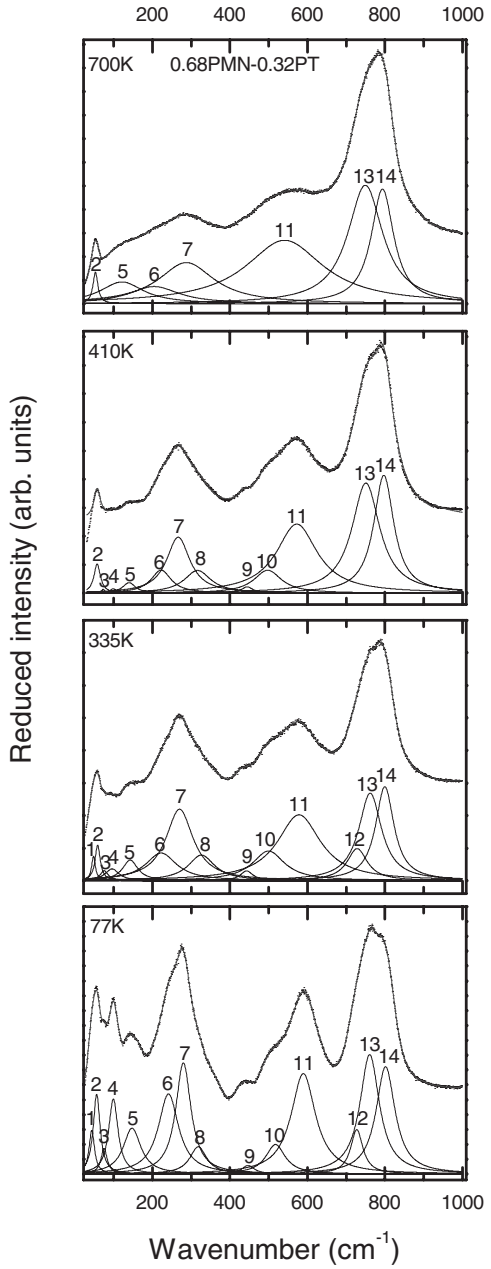

FIG. 12. Deconvolution of the Raman spectra of 0.68PMN-0.32PT at several selected temperatures. The numbers 1–14 label 14 Raman modes observed at 77 K. At high temperatures, this numeration is kept.

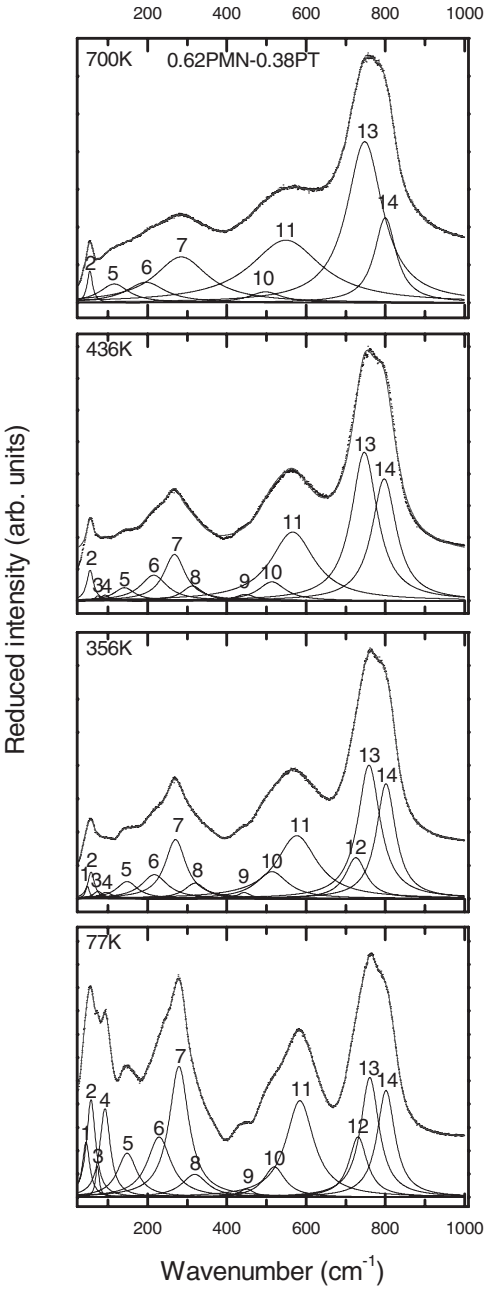

FIG. 13. Deconvolution of the Raman spectra of 0.62PMN-0.38PT at several selected temperatures. The numbers 1–14 label 14 Raman modes observed at 77 K. At high temperatures, this numeration is kept.

lines for the $R3m$ space group and 12 for the Pm one. Experimentally, we observed more lines, especially within the rhombohedral symmetry. In our opinion, there are two possible explanations of this clear discrepancy. The first one assumes that in these materials, the 1:1 order at the B-ion sublattice is still present, while the second one postulates the appearance of polar nanoregions with a lower symmetry than the rhombohedral one. Due to the 1:1 chemical order, similarly as in the case of PMN, the Raman spectra originate from the $R3m$ space group with $Z=2$, and according to the group theory analysis 16 lines are allowed. Kamba *et al.*[41] used such an explanation in order to interpret the Raman spectra of 0.71PMN-0.29PT. However, in our opinion the second explanation seems to be more probable.

We propose that the polar nanoregions of the monoclinic symmetry (Pm) strongly affect the Raman spectra collected within the rhombohedral one. Therefore, the observed Raman lines come from the coexistence of the rhombohedral and monoclinic symmetries. The presence of the monoclinic polar nanoregions in the rhombohedral matrix in the case of 0.72PMN-0.28PT is not surprising. It is highly probable that the nucleation of such nanoregions begins at high temperatures. The presence of the diffuse scattering and the parameters determined from the crystal structure refinements (Table I) confirm their existence. With the decrease in tem-

perature, they grow and thus are detected by the x-ray diffraction below 273 K as the long range monoclinic symmetry. It is worth noting that we also suggest the existence of the monoclinic polar nanoregions for 0.79PMN-0.21PT in spite of the fact that from the x-ray diffraction point of view this material does not exhibit a monoclinic symmetry. The high similarity of its Raman spectra to those recorded in the case of 0.72PMN-0.28PT as well as the obtained dielectric and structural results show that such an assumption is not unfounded. The 0.79PMN-0.21PT exhibits the relaxor behavior, which indicates that it is not homogeneous. For this material, the existence of diffuse scattering is detected not only within the cubic symmetry but also below the cubic-rhombohedral structural phase transition. Moreover, the intensities of the diffuse scattering grow with the decrease in temperature and reach the highest values at 12 K (Fig. 3). For this material, one of the highest values of the agreement factors R_{Bragg} and R_F as well as of the isotropic thermal parameters $B_{\mathrm{Pb}}^{\mathrm{iso}}$ (Table I) were determined. It is noteworthy that the temperature and composition dependences of the Raman linewidths, which will be discussed in detail in Sec. IIB3, also point to the presence of the polar monoclinic nanoregions within the rhombohedral symmetry. Therefore, basing on our complementary results, we suggest that the origin and the temperature evolution of the Raman spectra both for 0.79PMN-0.21PT and 0.72PMN-0.28PT are the effects of the coexistence of the cubic ($Pm\bar{3}m$) and rhombohedral ($R3m$) phases at high temperatures and of the rhombohedral ($R3m$) and monoclinic (Pm) ones at low temperatures.

Figures 12 and 13 show the deconvolutions of the Raman spectra of 0.68PMN-0.32PT and 0.62PMN-0.38PT, respectively. At 700 K, the Raman spectra can be well decomposed into seven lines for 0.68PMN-0.32PT and into eight lines in the case of 0.62PMN-0.38PT. As it has already been proposed, these high temperature Raman spectra may originate from the polar nanoregions with the tetragonal symmetry ($P4mm$). Below 600 K the splitting of the Raman lines and the appearance of new ones are observed. The most significant changes in the Raman spectra are detected near the structural phase transition from the cubic to the tetragonal symmetry, i.e., at 423 K in the case of 0.68PMN-0.32PT and at 460 K for 0.62PMN-0.38PT. These Raman spectra change only slightly during the second phase transitions from the tetragonal ($P4mm$) to the monoclinic (Pm) symmetry observed for 0.68PMN-0.32PT as well as from the tetragonal ($P4mm$) to the region of the tetragonal and monoclinic ($P4mm+Pm$) phases coexistence characteristic of 0.62PMN-0.38PT. We suggest that the best solution would be to decompose the spectra of both materials recorded within the tetragonal symmetry into 12 lines, while those collected within the monoclinic or monoclinic+tetragonal into 14 lines. It is worth noting that the Raman spectra characteristic of the pure monoclinic symmetry and those from the region where the monoclinic and tetragonal phases coexist exhibit the same number and sequences of Raman lines. The group theory analysis allows for the presence of 8 and 12 active Raman lines for the $P4mm$ and the Pm space groups, respectively. Hence, we again observed more lines than the group theory predicts. It seems reasonable to explain this discrepancy by the existence of polar nanoregions of the monoclinic symmetry already present within the tetragonal one. These monoclinic polar nanoregions affect the Raman spectra recorded within the tetragonal symmetry. Therefore, the Raman scattering data point to the coexistence of the tetragonal and monoclinic symmetries for both materials even if the x-ray diffraction shows such a coexistence only for 0.62PMN-0.38PT. It must be stressed that in the case of 0.68PMN-0.32PT, diffuse scattering is observed within the tetragonal symmetry and together with the results of the crystal structure refinements confirm the presence of these monoclinic nanoregions. Therefore, the origin and the temperature evolutions of the Raman spectra of 0.68PMN-0.32PT and 0.62PMN-0.38PT result from the coexistence of the cubic ($Pm\bar{3}m$) and tetragonal ($P4mm$) phases at high temperatures, while at lower temperatures they result from the coexistence of the tetragonal ($P4mm$) and monoclinic (Pm) symmetries.

Our explanation of the origin of the Raman spectra in the PMN-PT system may arouse doubts since for each of the characteristic symmetries, we observed more lines than the group theory predicts. Naturally, it is rather naive to expect a very good compatibility with the theoretical prediction in the case of such disordered materials as PMN-PT. Actually, the Raman scattering confirms the fact that the crystal structures determined from the x-ray diffraction studies are only average ones. Raman spectroscopy, being sensitive to the local symmetry, makes it possible to detect the presence of the 1:1 order in the B-ion sublattice as well as the coexistence of distinct phases with different lengths of coherence. It is interesting that in the investigated $(1-x)$PMN-xPT, we already observed the presence of the monoclinic symmetry for the solid solution where x is equal to 0.21. Moreover, as we showed in our previous paper,[52] the existence of the local monoclinic symmetry was even detected in the case of 0.91PMN-0.09PT below 200 K. These results seem to suggest that the correlated ion off-center displacements lead to the monoclinic symmetry and the rhombohedral or tetragonal phases are only a transitional state. Studies so far showed that the monoclinic symmetry becomes a long range property only for solid solutions with high PT contents and at low temperatures. Therefore, our x-ray diffraction studies point to the average rhombohedral or tetragonal symmetries. However, it is due to the Raman scattering that the existence of the monoclinic polar nanoregions can be observed. A similar conclusion was proposed by Glazer *et al.*[62] for PZT solid solutions and by Haumont *et al.*[63] for $PbSc_{1/2}Nb_{1/2}0_3$-$PbTiO_3$. Both groups of authors suggested that the local monoclinic order exists in the rhombohedral and tetragonal phases, which makes the morphotropic phase region more extended. Our results showed that this monoclinic symmetry never does not exist as a single phase. This is in good agreement with the studies of Noheda *et al.*,[6] who showed that the monoclinic phase is accompanied by the presence of a minority of rhombohedral or tetragonal phases. Finally, it must be stressed that the model of the local monoclinic symmetry is not the only one which appears in the literature of PMN-PT. For example, Xu *et al.*[17] suggested the existence of orthorhombic local symmetry due to the ⟨110⟩

polarization correlated in the short range. Vakrushev *et al.*[64] postulated the presence of the local strain field in PMN with the tetragonal type local symmetry.

3. Temperature and composition dependences of the Raman line parameters

The results of our calculations, namely, the temperature dependences of wave numbers ω, reduced intensities I, and linewidths Γ for the investigated crystals are presented in Figs. 14–17. The modes are labeled according to the deconvolutions of the Raman spectra at 77 K (Figs. 9–13) and the dotted lines mark the temperatures of phase transition determined from x-ray studies. It can be seen that near these temperatures, significant changes in ω, I, and Γ are observed. These changes are manifested by the departures from the linear behavior, the achievement of the minimal or maximal values, as well as by the disappearance of some Raman lines.

The temperature dependences of the Raman line frequencies are plotted in Fig. 14. In general, the frequencies of particular lines do not vary much for the studied PMN-PT materials. However, some lines exhibit a small temperature sensitivity. Usually when the temperature increases, the frequencies of the stretching vibrations decrease while the frequencies of the bending ones increase. This classical behavior is observed in the investigated PMN-PT solid solutions. For example, with increasing temperature, the line near 280 cm^{-1} is shifted toward higher frequencies, while the line near 600 cm^{-1} is shifted toward lower ones. Additionally, for some lines the shifts or departures from the linear behavior appear near the structural phase transitions. It can be seen in the case of lines 3 and 4 for both 0.72PMN-0.28PT and 0.68PMN-0.32PT. This can be connected to the different atomic arrangements attributed to the changes in the crystal symmetry.

It is noteworthy that the results of neutron scattering show the existence of the ferroelectric soft mode in PMN.[65,66] With the decrease in temperature, this transverse optic mode softens. It becomes overdamped near T_d and finally recovers below 220 K. The temperature dependences of the wave numbers of the Raman lines from the low frequency region as in previous studies[33–43] do not exhibit any softening or overdamping of the lines in the investigated materials.

The composition dependences of the wave numbers at 77 K are shown in Fig. 15. The frequencies of most modes are almost constant. However, some lines show a significant dependence on the PT content. For example, the lines near 150 and 280 cm^{-1} are shifted toward higher frequencies with the increase in Ti. This means that these lines are related to the vibrations of the B ions. The mass of the titanium is smaller than the average mass of the magnesium and niobium ions. Therefore, in the case of the solid solutions with higher PT contents, the shifts of the line frequencies to higher values are expected.

The temperature dependences of the reduced intensities of Raman lines are very similar for all of the investigated PMN-PT crystals and therefore Fig. 16 shows these dependences only for selected samples. It can be clearly seen that within a particular composition, most of the lines show similar temperature evolution, namely, intensities achieve the maxima or minima near the phase transition temperatures. These features might be related to changes in the crystal structure that influence the optical and dielectric properties of the investigated crystal. In addition, the intensities of the Raman lines also depend on the domain structure, which changes during the phase transitions.

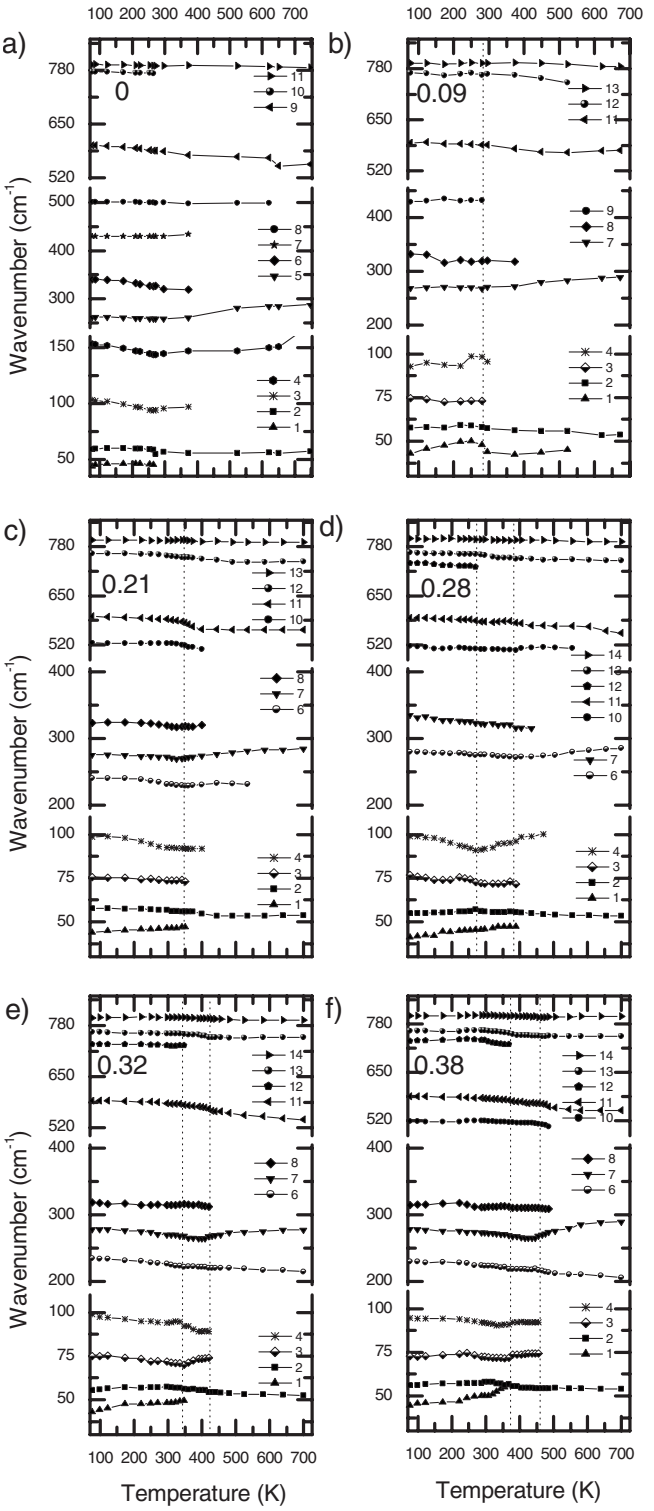

FIG. 14. Temperature dependences of the frequencies of Raman lines for (a) PMN, (b) 0.91PMN-0.09PT, (c) 0.79PMN-0.21PT, (d) 0.72PMN-0.28PT, (e) 0.68PMN-0.32PT, and (f) 0.62PMN-0.38PT.

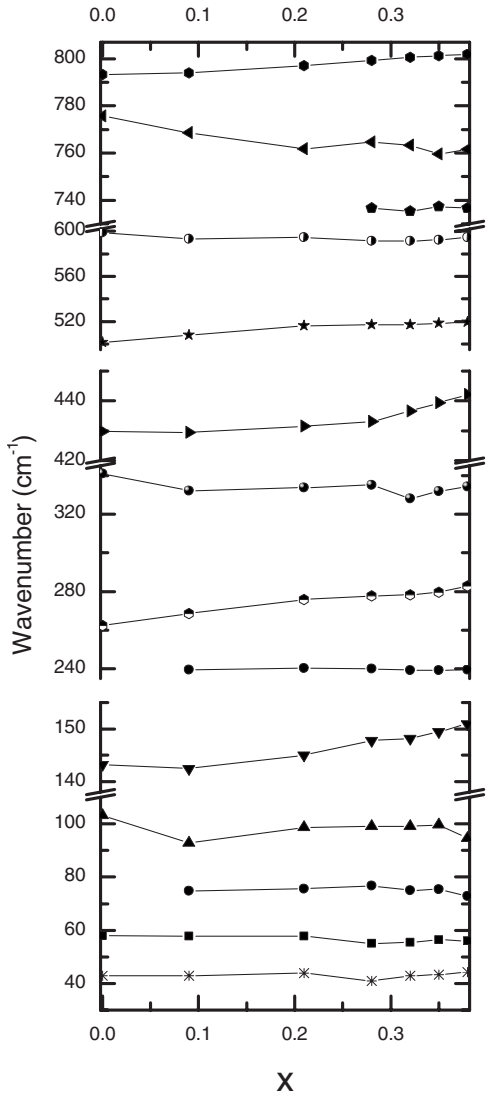

FIG. 15. Composition dependences of the frequencies of Raman lines for $(1-x)$PMN-xPT $(0 \leq x \leq 0.38)$ at 77 K.

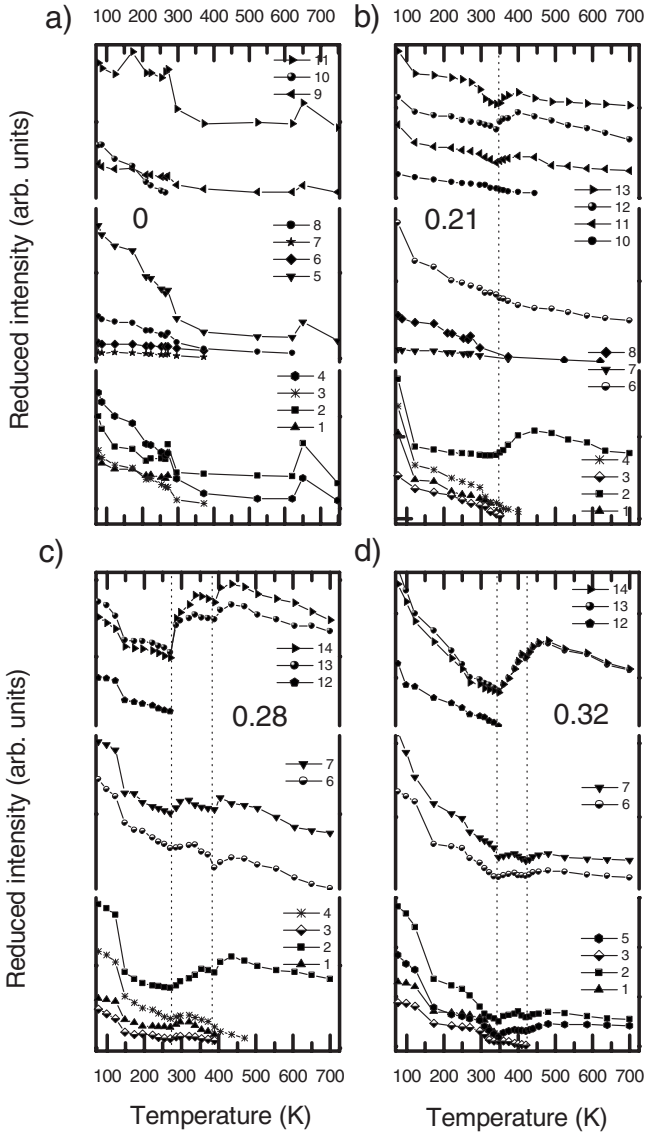

FIG. 16. Temperature dependences of the intensities of Raman lines for (a) PMN, (b) 0.79PMN-0.21PT, (c) 0.72PMN-0.28PT, and (d) 0.68PMN-0.32PT.

The temperature dependences of the linewidths for the PMN-PT solid solutions are presented in Fig. 17. For all of the investigated crystals, the Raman lines are very broad, even at 77 K. In general, the temperature evolution of the line width is attributed to the anharmonic effects.[46,66] For ordered materials, Γ decreases with the decrease in temperature and finally at 0 K its value should be negligible.[67] In the case of PMN-PT, the temperature evolutions of the linewidths are mainly determined by both the chemical disorder in the B sublattice and the static or dynamic local inhomogeneities related to the off-centered ion displacements correlated for different scales.

The linewidths of particular Raman lines exhibit different temperature and composition dependences. The intermediate and high frequency modes for all of the investigated compounds show the almost classical temperature evolution, namely, their linewidths decrease with decreasing temperature. However, the values of their linewidths at 77 K are still very high.

The linewidths of the low frequency modes exhibit nonclassical, anomalous temperature evolution. Namely, for pure PMN and the studied PMN-PT, we can distinguish regions where the linewidths increase with the decrease in temperature. For example, the width of line 2 (50 cm^{-1}) of pure PMN starts to increase at the Burns temperature and this increasing tendency is maintained up to 77 K. In the case of 0.72PMN-0.28PT, the width of the same line also starts to grow below 600 K and exhibits two maxima in the vicinity of the structural phase transition. A similar phenomenon, i.e., linewidth deviation from anharmonic background above the phase transition temperature, was observed for other complex perovskites, such as PST[46] and PIN,[48] exhibiting a different state of order and also for completely ordered PMW.[68] This, together with the fact that such a behavior was observed for all of our crystals, i.e., having a different composition and hence a different state of the B-site order, suggests that this Γ anomaly is not related to the disorder in the B-ion sublattice. This behavior, which is common in the lead-based complex perovskites, seems to originate from the ion off-

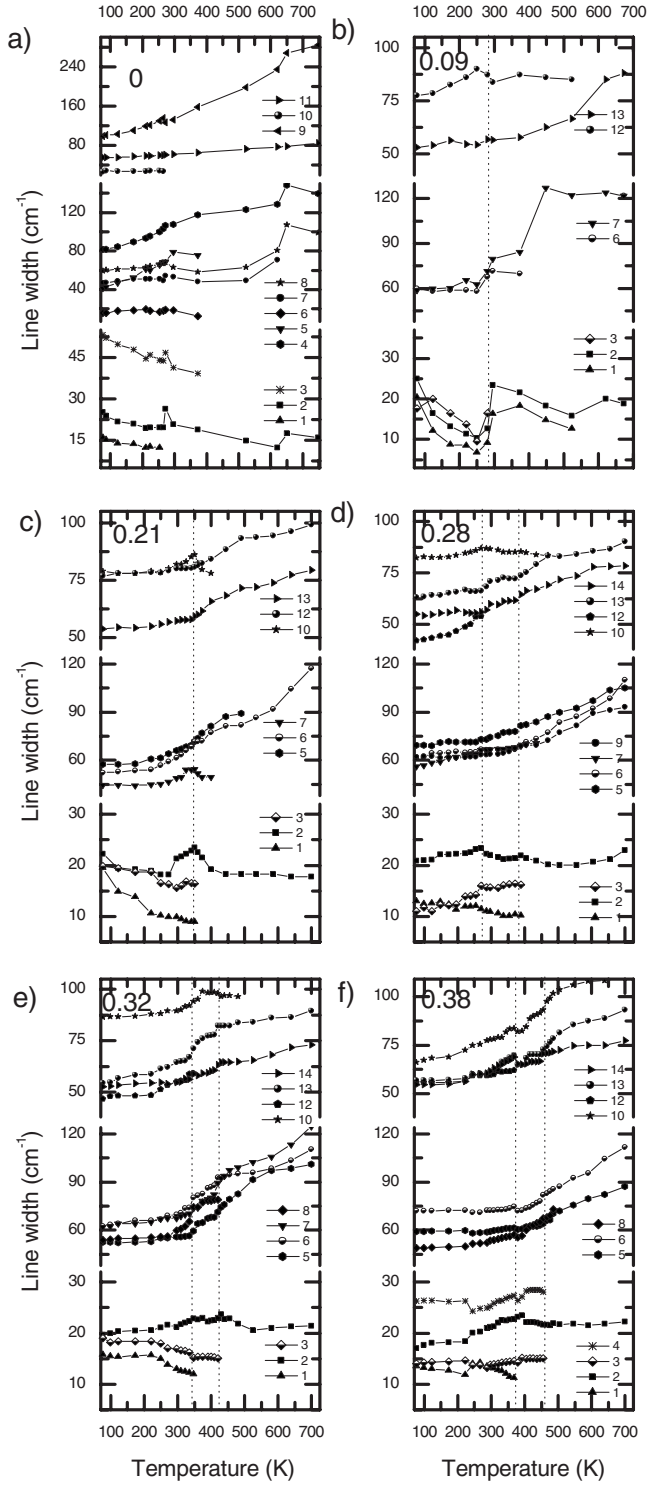

FIG. 17. Temperature dependences of the widths of Raman lines for (a) PMN, (b) 0.91PMN-0.09PT, (c) 0.79PMN-0.21PT, (d) 0.72PMN-0.28PT, (e) 0.68PMN-0.32PT, and (f) 0.62PMN-0.38PT.

centered displacements correlated for the short range scale. In addition, this Γ anomaly can be clearly seen for low frequency lines attributed to the Pb ions vibrations,[33,59] which shows that the origin of this phenomenon is connected to the Pb ion dynamics. Numerous neutron, x-ray, and EXAFS experiments show that Pb ions are randomly distributed over a sphere centered on the Pb special Wyckoff position in the lead-based complex perovskites[15,16,23,69] and even in the classical ferroelectric $PbTiO_3$.[70] The results of our crystal structure refinements also point to the disorder related to the Pb ions. Therefore, these complementary results show that the Pb ion dynamics play a key role in the phase transition mechanism.

In the case of low frequency linewidths, another important phenomenon is observed, namely, from about 200 to 77 K the widths of lines 1 and 2 surprisingly increase. It is noteworthy that this phenomenon, which in our opinion is crucial for the understanding of the physics of the PMN-PT system that can only be detected after calculations, was earlier known only for PMN.[38] It must be stressed that this phenomenon is strongly dependent on the composition and is observed only in the case of PMN and the solid solutions with $x \leq 0.21$. Such a broadening of these lines suggests that with decreasing temperature, the rhombohedral symmetry does not develop but further ion displacements correlated for the short range scale occur. The existence of further ion displacements, Ti/Mg/Nb toward the [111] direction and Pb correlated along the {100} direction, resulting in the appearance of the monoclinic local symmetry was proposed in the case of 0.9PMN-0.1PT by Dkhil *et al.*[16] and in our previous paper.[52] These anomalous temperature evolutions of the linewidth point to the appearance of a new, short range ordered phase and therefore seem to confirm our interpretation of the temperature evolutions of the Raman spectra based on the presence of the monoclinic nanoregions. This explanation seems to be plausible since in the case of 0.72PMN-0.28PT, in which according to x-ray data the monoclinic symmetry appears below 270 K, this phenomenon is not yet observed.

Our results suggest that the new symmetry in each stage is the result of the growth of clusters with a lower symmetry. The x-ray diffraction sensitive only to the long range order is unable to detect the presence of such polar nanoregions. Therefore, the data of the Raman scattering acting as a local probe are of great importance since the physics of the PMN-PT system takes place at nanoscale.

IV. CONCLUSION

$(1-x)$PMN-xPT solid solutions where x is 0, 0.09, 0.21, 0.28, 0.32, 0.35, and 0.38 were investigated by x-ray, dielectric, and Raman scattering techniques. The results of our complementary studies made it possible to present the phase diagram of this system. The increase in Ti content gradually changes the properties of the PMN-PT materials. Consequently, the relaxor behavior transforms into the ferroelectric one and structural phase transitions of different types occur. The room temperature symmetry transforms from the pseudocubic ($Pm\bar{3}m$) specific for PMN to the rhombohedral ($R3m$) and then to the monoclinic (Pm) one in the vicinity of the MPB. However, very high values of the reliability factors and the isotropic thermal factors of Pb ions determined from the crystal structure refinements show that all these symmetries are only average.

For all of the investigated crystals, the Raman spectra are observed in the whole measured temperature range, even

within the paraelectric cubic phase. In the case of pure PMN and the solid solutions with Ti contents $x \leq 0.09$, the 1:1 chemical order in the *B*-ion sublattice leads to the appearance of clusters with $Fm\bar{3}m$ symmetry. This, in turn, is responsible for the presence of the high temperature Raman spectrum. In the case of solid solutions with higher PT contents, we postulate that their Raman spectra originate from the polar nanoregions of the rhombohedral ($R3m$) or the tetragonal ($P4mm$) symmetry. With the decrease in temperature, the splitting and narrowing of the Raman lines occur. This together with the characteristic behavior observed in the temperature dependences of frequencies, reduced intensities, and linewidths point to the changes in the crystal symmetry. The deconvolutions of the Raman spectra reveal that for each of the characteristic symmetries, more lines than the group theory analysis predicts were observed. These discrepancies can be explained by the fact that PMN-PT are highly disordered, inhomogeneous materials in which coexistence of different phases occur. Our Raman scattering results show that the crystal symmetries determined from the x-ray diffraction play the role of a matrix in which the polar nanoregions with distinct local symmetry are embedded. In most of the investigated PMN-PT crystals, the presence of the local monoclinic symmetry was detected. This suggests that the monoclinic symmetry is preferred in this system while the rhombohedral or tetragonal ones are only transition states. The temperature dependences of the Raman linewidths related to the Pb vibrations point to the special role of Pb ions dynamics in the mechanism of phase transitions. It seems that each change in the symmetry originates from the correlated ion off-center displacements. These correlated displacements cause the nucleation of regions with different local symmetries, which can grow with the decrease in temperature. The Raman scattering is capable of revealing their presence due to its sensitivity to the local order even if they are not large enough to be detected by x-ray diffraction. Therefore, in our opinion, the studies of local phenomena by the Raman scattering are essential to understand the complex behavior of the PMN-PT system.

*Author to whom correspondence should be addressed.

[1] L. E. Cross, Ferroelectrics **76**, 241 (1987).
[2] S. E. Park and T. R. Shrout, J. Appl. Phys. **82**, 1804 (1997).
[3] H. Fu and R. H. Cohen, Nature (London) **403**, 281 (2000).
[4] S. W. Choi, T. R. Shrout, S. J. Jang, and A. S. Bhalla, Ferroelectrics **100**, 29 (1989).
[5] O. Noblanc, P. Gaucher, and G. Calvarin, J. Appl. Phys. **79**, 4291 (1996).
[6] B. Noheda, D. E. Cox, G. Shirane, Z.-G. Ye, and J. Gao, Phys. Rev. B **66**, 054104 (2002).
[7] P. M. Gehring, W. Chen, Z. G. Ye, and G. Shirane, J. Phys.: Condens. Matter **16**, 7113 (2004).
[8] D. Zekria, V. A. Shuvaeva, and A. M. Glazer, J. Phys.: Condens. Matter **17**, 1593 (2005).
[9] V. A. Shuvaeva, A. M. Glazer, and D. Zekria, J. Phys.: Condens. Matter **17**, 5709 (2005).
[10] Z. G. Ye, Y. Bing, J. Gao, A. A. Bokov, P. Stephens, B. Noheda, and G. Shirane, Phys. Rev. B **67**, 104104 (2003).
[11] P. Bonneau, P. Garnier, G. Calvarin, E. Husson, J. R. Gavarri, A. W. Heiwat, and A. Morell, J. Solid State Chem. **91**, 350 (1991).
[12] N. Takesue, Y. Fujii, and H. You, Phys. Rev. B **64**, 184112 (2001).
[13] H. You and Q. M. Zhang, Phys. Rev. Lett. **79**, 3950 (1997).
[14] D. M. Fanning, I. K. Robinson, S. T. Young, E. V. Colla, D. D. Viehland, and D. A. Payne, J. Appl. Phys. **87**, 840 (2000).
[15] N. de Mathan, E. Husson, G. Calvarin, J. R. Gavarri, A. W. Hewat, and A. Morell, J. Phys.: Condens. Matter **3**, 8159 (1991).
[16] B. Dkhil, J. M. Kiat, G. Calvarin, G. Baldinozzi, S. B. Vakhrushev, and E. Suard, Phys. Rev. B **65**, 024104 (2001).
[17] G. Xu, G. Shirane, J. R. D. Copley, and P. M. Gehring, Phys. Rev. B **69**, 064112 (2004).
[18] K. Hirota, Z. G. Ye, S. Wakimoto, P. M. Gehring, and G. Shirane, Phys. Rev. B **65**, 104105 (2002).
[19] P. K. Davies and M. A. Akbas, J. Phys. Chem. Solids **61**, 159 (2000).
[20] J. Chen, H. M. Chan, and M. P. Harmer, J. Am. Ceram. Soc. **72**, 593 (1989).
[21] Y. Yan, S. J. Pennycook, Z. Xu, and D. Viehland, Appl. Phys. Lett. **72**, 3145 (1998).
[22] G. Burns and F. H. Dacol, Phys. Rev. B **28**, 2527 (1983).
[23] E. Prouzet, E. Husson, N. de Mathan, and A. Morell, J. Phys.: Condens. Matter **5**, 4889 (1993).
[24] R. Blinc, A. Gregorovic, B. Zalar, R. Pirc, V. V. Laguta, and M. D. Glinchuk, Phys. Rev. B **63**, 024104 (2000).
[25] D. Vanderbilt and M. H. Cohen, Phys. Rev. B **63**, 094108 (2001).
[26] F. Bai, N. Wang, J. Li, D. Viehland, P. Gehring, G. Xu, and G. Shirane, J. Appl. Phys. **96**, 1620 (2004).
[27] H. Cao, F. Bai, J. Li, D. Viehland, P. Gehring, G. Xu, H. Hiraka, and G. Shirane, J. Appl. Phys. **97**, 094101 (2005).
[28] G. Shirane, R. Pepinsky, and B. C. Frazer, Acta Crystallogr. **9**, 131 (1956).
[29] G. Xu, D. Viehland, J. F. Li, P. M. Gehring, and G. Shirane, Phys. Rev. B **68**, 212410 (2003).
[30] A. K. Singh and D. Pandey, Phys. Rev. B **67**, 064102 (2003).
[31] B. Guttler, B. Mihailova, R. Stosch, U. Bismayer, and M. Gospodin, J. Mol. Struct. **661-662**, 469 (2003).
[32] A. Ratuszna, Ph. Daniel, J. Kapusta, and M. Rousseau, Phys. Rev. B **57**, 10470 (1998).
[33] E. Husson, L. Abello, and A. Morell, Mater. Res. Bull. **25**, 539 (1990).
[34] I. G. Siny, S. G. Lushnikov, R. S. Katiyar, and V. N. Schmidt, Ferroelectrics **226**, 191 (1999).
[35] I. G. Siny, S. G. Lushnikov, R. S. Katiyar, and E. A. Rogacheva, Phys. Rev. B **56**, 7962 (1997).
[36] F. Jiang, S. Kojima, Ch. Zhao, and Ch. Feng, J. Appl. Phys. **88**, 3608 (2000).
[37] F. Jiang, S. Kojima, Ch. Zhao, and Ch. Feng, Appl. Phys. Lett. **79**, 3938 (2001).

[38] O. Svitelskiy, J. Toulouse, G. Yong, and Z. G. Ye, Phys. Rev. B **68**, 104107 (2003).
[39] H. Idink and W. White, J. Appl. Phys. **76**, 1789 (1994).
[40] M. El. Marssi, R. Farhi, and Yu. Yuzyuk, J. Phys.: Condens. Matter **10**, 9161 (1998).
[41] S. Kamba, E. Buixaderas, J. Petzelt, J. Fousek, J. Nosek, and P. Bridenbaugh, J. Appl. Phys. **93**, 933 (2003).
[42] B. Chaabane, J. Kreisel, P. Bouvier, G. Lucazeau, and B. Dkhil, Phys. Rev. B **70**, 134114 (2004).
[43] H. Ohwa, M. Iwata, H. Orihara, N. Yasuda, and Y. Ishibashi, J. Phys. Soc. Jpn. **70**, 3149 (2001).
[44] A. Lebon, M. El. Marssi, R. Farhi, H. Dammak, and G. Calvarin, J. Appl. Phys. **89**, 3947 (2001).
[45] J. Toulouse, F. Jiang, O. Svitelskiy, W. Chen, and Z. G. Ye, Phys. Rev. B **72**, 184106 (2005).
[46] U. Bismayer, V. Devarajan, and P. Groves, J. Phys.: Condens. Matter **1**, 6977 (1989).
[47] C. Boulesteix, C. Caranoni, C. Z. Kang, L. S. Sapozhnikova, I. G. Siny, and T. A. Smirnova, Ferroelectrics **107**, 241 (1990).
[48] A. Kania, K. Roleder, G. E. Kugel, and M. Hafid, Ferroelectrics **135**, 75 (1992).
[49] M. Iwata, N. Tomisato, H. Orihara, N. Arai, N. Tanaka, H. Ohwa, N. Yasuda, and Y. Ishibashi, Jpn. J. Appl. Phys., Part 1 **40**, 5819 (2001).
[50] S. Kim, I. S. Yang, J. K. Lee, and K. S. Hong, Phys. Rev. B **64**, 094105 (2001).
[51] O. Svitelskiy, D. La-Orauttapong, J. Toulouse, W. Chen, and Z. G. Ye, Phys. Rev. B **72**, 172106 (2005).
[52] A. Slodczyk, A. Kania, Ph. Daniel, and A. Ratuszna, J. Phys. D **38**, 2910 (2005).
[53] A. Kania, A. Slodczyk, and Z. Ujma, J. Cryst. Growth **289**, 134 (2006).
[54] A. K. Singh and D. Pandey, J. Phys.: Condens. Matter **13**, L931 (2001).
[55] J. M. Kiat, Y. Uesu, B. Dkhil, M. Matsuda, Ch. Malibert, and G. Calvarin, Phys. Rev. B **65**, 064106 (2002).
[56] C. Malibert, B. Dkhil, J. M. Kiat, D. Durand, J. F. Berar, and A. Spasojevic-de-Bire, J. Phys.: Condens. Matter **9**, 7485 (1997).
[57] N. Lampis, P. Sciau, and A. Geddo Lehmann, J. Phys.: Condens. Matter **11**, 3489 (1989).
[58] A. Kania, E. Talik, M. Kruczek, and A. Slodczyk, J. Phys.: Condens. Matter **17**, 6737 (2005).
[59] S. A. Prosandeev, E. Cockayne, P. B. Burton, S. Kamba, J. Petzelt, Yu. Yuzyuk, R. S. Katiyar, and S. B. Vakhrushev, Phys. Rev. B **70**, 134110 (2004).
[60] C. A. Randall, A. S. Bhalla, T. R. Shrout, and L. E. Cross, J. Mater. Res. **5**, 829 (1990).
[61] B. P. Burton and E. Cockayne, Phys. Rev. B **60**, R12542 (1999).
[62] A. M. Glazer, P. A. Thomas, K. Z. Baba-Kishi, G. K. H. Pang, and C. W. Tai, Phys. Rev. B **70**, 184123 (2004).
[63] R. Haumont, P. Gemeiner, B. Dkhil, J. M. Kiat, and A. Bulou, Phys. Rev. B **73**, 104106 (2006).
[64] S. B. Vakrushev, A. Ivanov, and J. Kulda, Phys. Chem. Chem. Phys. **7**, 2340 (2005).
[65] P. M. Gehring, S. Wakimoto, Z. G. Ye, and G. Shirane, Phys. Rev. Lett. **87**, 277601 (2001).
[66] S. Wakimoto, C. Stock, R. J. Birgeneau, Z. G. Ye, W. Chen, W. J. L. Buyers, P. M. Gehring, and G. Shirane, Phys. Rev. B **65**, 172105 (2002).
[67] C. Carabatos-Nedelec and P. Becker, J. Raman Spectrosc. **28**, 663 (1998).
[68] A. Kania, E. Jahfe, G. E. Kugel, K. Roleder, and M. Hafid, J. Phys.: Condens. Matter **8**, 4441 (1996).
[69] G. Baldinozzi, P. Sciau, and J. Lapasset, Phys. Status Solidi A **133**, 17 (1992).
[70] J. Kwapulinski, M. Pawelczyk, and J. Dec, Ferroelectrics **192**, 307 (1997).